

Short wavelength (4 μm) quantum cascade detector based on strain compensated InGaAs/InAlAs

F. R. Giorgetta,^{1,a)} E. Baumann,¹ R. Théron,¹ M. L. Pellaton,¹ D. Hofstetter,¹ M. Fischer,² and J. Faist²

¹University of Neuchâtel, A.-L. Breguet 1, CH-2000 Neuchâtel, Switzerland

²ETH Zürich, Wolfgang-Pauli Strasse 16, CH-8092 Zurich, Switzerland

We report on a quantum cascade detector based on nearly strain compensated InGaAs/InAlAs pseudomorphically grown on InP substrate and detecting light at short wavelengths around 4 μm . The background limited infrared performance (BLIP) condition is met at a temperature of 108 K with a high detectivity of $D_{\text{BLIP}}^* = 1.2 \times 10^{11}$ Jones.

Fast commercial semiconductor interband photodetectors are common at wavelengths up to about 1.6 μm . At longer wavelengths, intersubband (ISB) photodetectors are promising candidates for fast light detection; their operating speed is intrinsically limited by the electron ISB scattering time which lies in the range of 1 ps. Short response times have already been reported for quantum well infrared photodetectors (QWIPs) and for quantum cascade detectors (QCDs), detecting at frequencies up to 82 GHz at 10 μm ,¹ respectively, 23 GHz at 5 μm .² Those devices were grown with the mature, lattice matched GaAs/Al_xGa_{1-x}As and In_{0.53}Ga_{0.47}As/In_{0.52}Al_{0.48}As system, respectively.

The most common ISB photodetector design is the photoconductive (PC) QWIP. Photovoltaic (PV) ISB detectors include the PV QWIP, as demonstrated by Schneider *et al.*,³ and the QCD. Since most QWIPs rely on the first excited state being close to the continuum, a given material composition imposes a very specific transition energy. In contrast, the QCD, which uses a bound-to-bound transition, can be designed at any energy up to a certain limit, and does therefore not suffer from this constraint. The first PV ISB photodetectors based on a quantum cascade were demonstrated by Graf *et al.*⁴ and by Gendron *et al.*,⁵ who coined the term QCD. The absence of dark current in QCDs leads to several advantages compared to PC-QWIPs. There is no dark current noise. The integration time in readout circuits can be extended, since no dark current saturates the readout capacitance. Also, the thermal load of the detector is reduced, which is of interest if the available cooling is limited, for example, in space born systems or handheld terrestrial staring systems.

The upper limit of the ISB transition energy in a particular material system is determined by the conduction band offset (CBO) between quantum well (QW) and barrier. The CBO for lattice matched In_{0.53}Ga_{0.47}As/In_{0.52}Al_{0.48}As amounts to 520 meV. The shortest ISB wavelength is obtained if the first excited state of the QW is close to the continuum; in this particular material system, the short wavelength limit is at roughly 4 μm . As QCDs rely on a bound-to-bound transition in the active QW, the shortest QCD detection wavelength becomes somewhat longer, namely, about 4.5 μm . By increasing the In content above 53% in the In-

GaAs QW and reducing it below 52% in the InAlAs barrier, the CBO can be increased. However, the modified In contents introduce strain between the barrier and QW layers and the InP substrate; since the strains are of opposite signs, namely, tensile in the barrier and compressive in the QW, a strain compensated pseudomorphic active region can be obtained by choosing appropriate layer thicknesses and material compositions. The QCD presented in this letter is based on strained In_{0.61}Ga_{0.39}As/In_{0.42}Al_{0.55}As with a CBO of 610 meV.⁶

The detector design presented here corresponds, in general, to the one described in Ref. 7. The active region consists of ten repetitions of a thick active QW A and a nominally undoped extraction cascade B-H, as seen in Fig. 1. The peak detection energy of the QCD, which corresponds to the ISB transition (ISBT) energy $A_1 \rightarrow A_2$ between ground and first state in QW A, was calculated to be 319 meV (3.88 μm) using a Schrödinger solver. The ground state of the first extractor QW B is in resonance with A_2 , ensuring efficient transport of photoexcited electrons into the extraction cascade through resonant tunneling. This allows for a thick barrier between the active QW A and the extractor, resulting in

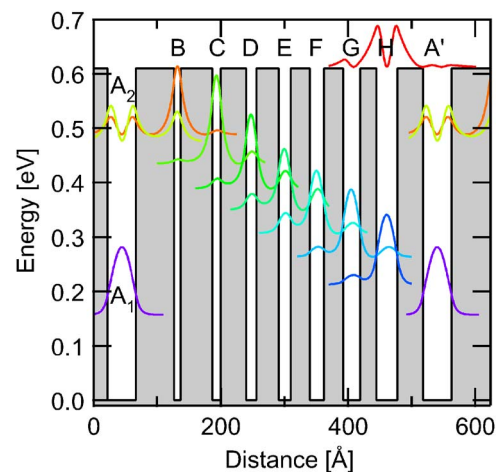


FIG. 1. (Color online) Simulated conduction band profile of the strain compensated In_{0.61}Ga_{0.39}As/In_{0.42}Al_{0.55}As QCD with a CBO of 610 meV designed for a detection energy of 319 meV. Starting with QW A from left to right, the layer thicknesses in angstroms are **45/60/10/50/13/40/16/35/19/30/22/30/27/26/33/40**; the In_{0.61}Ga_{0.39}As layers are in boldface.

^{a)}Electronic mail: fabrizio.giorgetta@unine.ch.

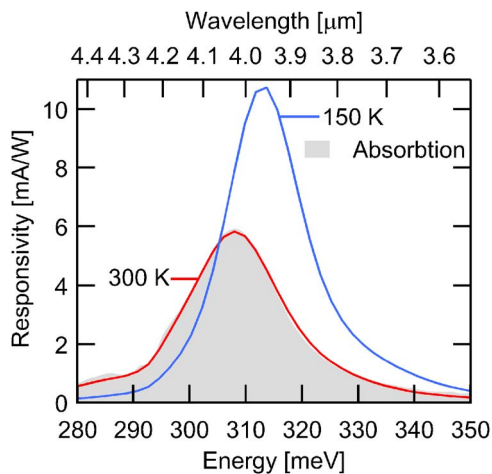


FIG. 2. (Color online) Responsivity spectra of the strained InGaAs QCD at 150 and 300 K, along with the absorption line shape measured at 300 K.

a higher device resistance and thus lower Johnson noise. To ensure a fast vertical transport of photoexcited carriers across the extractor, the energy separation between adjacent extractor ground states is close to the $\text{In}_{0.61}\text{Ga}_{0.39}\text{As}$ LO phonon energy of 34 meV. The $\text{In}_{0.61}\text{Ga}_{0.39}\text{As}$ QWs and $\text{In}_{0.42}\text{Al}_{0.55}\text{As}$ barriers with a lattice mismatch of $\pm 0.5\%$ toward the InP substrate offer a CBO of 610 meV. As the active region consists to 60% of barriers, the tensile strain of the barrier layers is not completely compensated by the compressive strain of the QW layers, wherefore the active region has a small residual strain of 0.1% toward the InP substrate. Taking into account this small lattice mismatch and the only 496 nm thick active region, the grown crystal is expected to remain pseudomorphic. Indeed, the wafer did not show any cracks.

Molecular beam epitaxy of the layer started with a 600 nm thick $\text{In}_{0.53}\text{Ga}_{0.47}\text{As}$ lower contact layer lattice matched to the InP substrate, followed by ten repetitions of the active region as depicted in Fig. 1; the layer thicknesses of one such period are given in the figure caption. The structure is capped by a 200 nm thick $\text{In}_{0.53}\text{Ga}_{0.47}\text{As}$ upper contact layer. Both contact layers and the active QWs A are n doped to $1 \times 10^{18} \text{ cm}^{-3}$ whereas the extractor is undoped.

For transmission and current responsivity measurements of this device, the sample edges were polished into 45° facets, as described in Ref. 7. For the current responsivity measurements, $(200 \mu\text{m})^2$ mesa were processed and contacted by a Ti/Ge/Au/Ti/Au metallization. Optical characterization was performed in a Fourier transform infrared spectrometer using a KBr beam splitter and glowbar illumination. In Fig. 2, the responsivity measured at 150 and 300 K along with the absorption line shape at 300 K is depicted. As expected for a QCD, the spectral line shape of the 300 K absorption and responsivity are nearly identical. At 5 K, the measured responsivity peaks at 318 meV ($3.90 \mu\text{m}$). This corresponds well to the simulated $A_1 \rightarrow A_2$ ISBT energy of 319 meV and demonstrates that both simulation and growth of strained InGaAs/InAlAs heterostructures have reached a high degree of maturity. The responsivity reaches a maximal value of 10.7 mA/W at 150 K. The top panel of Fig. 3 shows normalized responsivity spectra measured at device temperatures between 5 and 300 K. The bottom panel of Fig. 3 depicts the peak position and full width at half maximum (FWHM) extracted from a Lorentzian fit of the responsivity

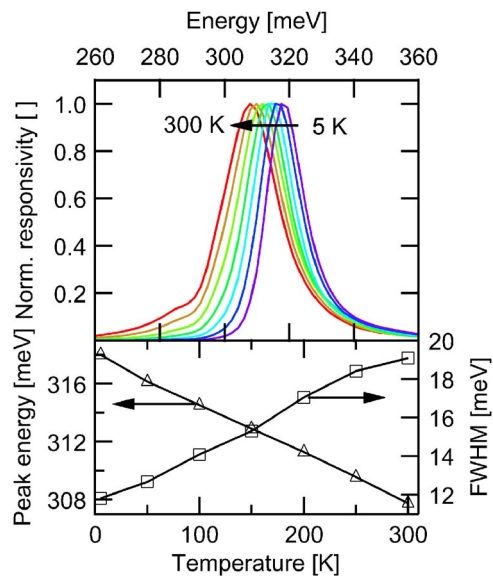


FIG. 3. (Color online) Temperature dependence of the responsivity line shape. Top panel: normalized responsivity spectra at 5, 50, 100, 150, 200, 250, and 300 K. Bottom panel: FWHM and peak responsivity energy extracted from a Lorentzian fit as function of temperature.

as function of device temperature. With increasing temperature, both responsivity and absorption spectra broaden and redshift. The redshift shows linear behavior with a slope of -0.034 meV/K . The shift as well as the broadening are explained by the temperature dependence of the Fermi-Dirac distribution of the electrons in QW A's ground state A_1 and the different nonparabolicities of the subbands A_1 and A_2 .⁸ At higher temperatures, the electron population in A_1 is smeared out over a certain energy range, which corresponds to an increasingly large range of k vectors. In conjunction with the nonparabolicities of the subbands, this results in a broadening and a noticeable redshift of the ISBT.

The Johnson noise limited detectivity D^* shown in Fig. 4 was calculated with the measured resistance-area product R_0A around 0 V also displayed in Fig. 4 and the peak responsivity. At 300 K, D^* equals 4.9×10^7 Jones. The background limited infrared performance (BLIP) detectivity D_{BLIP}^* is 1.2×10^{11} Jones for a 300 K background and a hemispherical field of view; it is reached at $T_{\text{BLIP}} = 108 \text{ K}$.

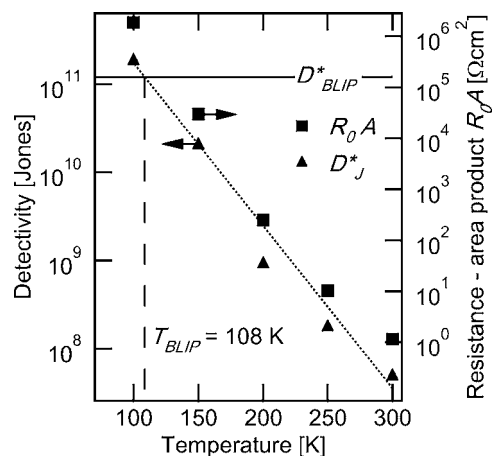


FIG. 4. Johnson noise limited detectivity D^* at different temperatures. D^* was obtained with the resistance area product R_0A (depicted on the right axis) measured around 0 V and the measured responsivity. D^* equals the background limited detectivity D_{BLIP}^* at $T_{\text{BLIP}} = 113 \text{ K}$.

These values compare favorably to other intersubband and interband photodetectors. For comparison, a $4\ \mu\text{m}$ $\text{In}_{0.53}\text{Ga}_{0.47}\text{As}/\text{In}_{0.52}\text{Al}_{0.48}\text{As}$ bound to continuum QWIP demonstrated by Hasnain *et al.*⁹ had a D_{BLIP}^* of 2.3×10^{10} Jones at 120 K. Commercial photovoltaic InSb detectors have typical D^* values of 7×10^{10} Jones at $4\ \mu\text{m}$ and 77 K.

In conclusion, the QCD detection energy range of the $\text{InGaAs}/\text{InAlAs}$ material system was extended toward higher energies by introducing 0.5% strain between QW/barrier and the InP substrate, while a high material quality was maintained. At 150 K, the presented $\text{In}_{0.61}\text{Ga}_{0.39}\text{As}/\text{In}_{0.45}\text{Al}_{0.55}\text{As}$ QCD peaks at $3.96\ \mu\text{m}$ with a responsivity of $10.7\ \text{mA/W}$. The BLIP condition is met at 108 K with a high $D_{\text{BLIP}}^* = 1.2 \times 10^{11}$ Jones. Thus, QCDs are promising candidates for low-level light detection around $4\ \mu\text{m}$. By further increasing the strain, $\text{InGaAs}/\text{InAlAs}$ QCDs can be realized at even shorter wavelengths. Faist *et al.*⁶ reported on a short wavelength quantum cascade laser based on $\text{In}_{0.7}\text{Ga}_{0.3}\text{As}/\text{In}_{0.4}\text{Al}_{0.6}\text{As}$ QW/barriers with a CBO of 740 meV. This system would allow for QCDs operating down to $2.9\ \mu\text{m}$ (up to 430 meV).

This work was financially supported by the Professorship Program and the National Center of Competence in Research “Quantum Photonics,” both financed from the Swiss National Science Foundation.

¹H. C. Liu and J. Li, Appl. Phys. Lett. **67**, 1594 (1995).

²D. Hofstetter, M. Graf, T. Aellen, J. Faist, L. Hvozدارa, and S. Blaser, Appl. Phys. Lett. **89**, 061119 (2006).

³H. Schneider, K. Kheng, M. Ramsteiner, J. D. Ralston, F. Fuchs, and P. Koidl, Appl. Phys. Lett. **60**, 1471 (1992).

⁴M. Graf, G. Scalari, D. Hofstetter, J. Faist, H. Beere, E. Linfeld, D. Ritchie, and G. Davies, Appl. Phys. Lett. **84**, 475 (2004).

⁵L. Gendron, M. Carras, A. Huynh, V. Ortiz, C. Koeniguer, and V. Berger, Appl. Phys. Lett. **85**, 2824 (2004).

⁶J. Faist, F. Capasso, D. L. Sivco, A. L. Hutchinson, S. G. Chu, and A. Y. Cho, Appl. Phys. Lett. **72**, 680 (1998).

⁷M. Graf, N. Hoyler, M. Giovannini, J. Faist, and D. Hofstetter, Appl. Phys. Lett. **88**, 241118 (2006).

⁸D. C. Larrabee, G. A. Khodaparast, J. Kono, K. Ueda, Y. Nakajima, M. Nakai, S. Sasa, M. Inoue, K. I. Kolokolov, J. Li, and C. Z. Ning, Appl. Phys. Lett. **83**, 3936 (2003).

⁹G. Hasnain, B. F. Levine, D. L. Sivco, and A. Y. Cho, Appl. Phys. Lett. **56**, 770 (1990).